Landau levels and shallow donor states in GaAs/AlGaAs multiple quantum wells at megagauss magnetic fields

M. Zybert, M. Marchewka, and E. M. Sheregii
Centre for Microelectronics and Nanotechnology, University of Rzeszów, Pigonia 1, 35-959 Rzeszów, Poland

D. G. Rickel, J. B. Betts, F. F. Balakirev, M. Gordon, A. V. Stier, and C. H. Mielke
National High Magnetic Field Laboratory, Los Alamos, New Mexico 87545, USA

P. Pfeffer and W. Zawadzki
Institute of Physics, Polish Academy of Sciences, Al. Lotników 02-668, Warsaw, Poland
(Received 2 November 2016; revised manuscript received 26 January 2017; published 27 March 2017)

Landau levels and shallow donor states in multiple GaAs/AlGaAs quantum wells (MQWs) are investigated by means of the cyclotron resonance at megagauss magnetic fields. Measurements of magneto-optical transitions were performed in pulsed fields up to 140 T and temperatures from 6–300 K. The 14×14 $\mathbf{P}\cdot\mathbf{p}$ band model for GaAs is used to interpret free-electron transitions in a magnetic field. Temperature behavior of the observed resonant structure indicates, in addition to the free-electron Landau states, contributions of magnetodonor states in the GaAs wells and possibly in the AlGaAs barriers. The magnetodonor energies are calculated using a variational procedure suitable for high magnetic fields and accounting for conduction band nonparabolicity in GaAs. It is shown that the above states, including their spin splitting, allow one to interpret the observed magneto-optical transitions in MQWs in the middle infrared region. Our experimental and theoretical results at very high magnetic fields are consistent with the picture used previously for GaAs/AlGaAs MQWs at lower magnetic fields.

DOI: 10.1103/PhysRevB.95.115432

I. INTRODUCTION

Magnetodonor states in semiconductors have been the subject of sustained experimental and theoretical interest due to their interesting physical properties, important use in infrared technology [1–12] and quantum computing [13]. Magneto-optical and magnetotransport investigations proved to be useful in determining positions of donors in multiple quantum wells (MQWs), which is important for device applications. It is of interest to verify for ultrahigh magnetic fields the applications of previous theoretical assumptions for properties of donor centers in both bulk crystals and QWs at small magnetic fields [3,5,6,8]. One of the important questions is the magnetic field dependence of the optical transition energies for the extreme field range.

In the case of the bulk GaAs crystals, the cyclotron resonance experiments in the ultrahigh magnetic fields were performed and interpreted using 7×7 band model [1,4,7]. This problem specifically concerns the MQWs based on the GaAs/AlGaAs heterostructures where the donor centers can exist both in the wells and barriers. In addition to the useful applications of MQWs to infrared photodetectors [14–17], light-emitting diode array (emitters) [18–21] and cascade lasers [22–25], nonlinear optics [26], phononic crystals [27] they provide a test system for the study of electron correlation in two dimensional electron gas (2DEG) when the electrons are spatially conned by the potentials of closely spaced multilayers [28–35].

In this paper we present results on the cyclotron resonance (CR) in the GaAs/AlGaAs MQWs containing residual Si donors both in the GaAs wells and AlGaAs barriers. The experimental data are obtained in a wide range of temperatures and in the megagauss magnetic fields. They are described using a sophisticated 14×14 band model for free-electron Landau levels and variational calculations for magnetodonors. The theory takes into account the nonparabolicity and nonsphericity of the conduction band in GaAs, which strongly influences all energies at the employed very strong magnetic fields. A connection with the results of other authors is made, both those of Brosak *et al.* [36] who used much lower constant fields, as well as those of Najda *et al.* [1] and W. Zawadzki *et al.* [7] where authors worked with very high pulsed fields similar to ours but for bulk GaAs crystals.

Experiment is performed using improved installation of the megagauss magnetic field generator [37] with a system of registration of magnetotransmission for both increasing and decreasing magnetic field with highly resolved data acquisition. This enables us to obtain reliable values of the resonance magnetic field.

II. EXPERIMENTAL RESULTS

Magneto-optical measurements in the infrared region and pulsed megagauss magnetic fields were performed at the National High Magnetic Field Laboratory, Pulsed Field Facility in Los Alamos. Magnetic fields up to 150 T were generated in a single-turn coil discharging a capacity of 250 kJ and inductance of 17.5 nH during 6 μs. The CR of electrons in the MQW, was excited with the CO_2 laser radiation at two different wavelengths: $\lambda_1 = 10.59\,\mu$m ($h\nu = 116.7$ meV) and $\lambda_2 = 9.69\,\mu$m ($h\nu = 128.0$ meV) with the power of about 80 mW for each wavelength. The magnetic field B was parallel to the crystal growth direction and maintained perpendicular to the two-dimensional electron gas plane with a special sample holder ensuring the Faraday geometry [37].

A HgCdTe detector was used to detect the radiation transmitted through the sample placed within the single-turn

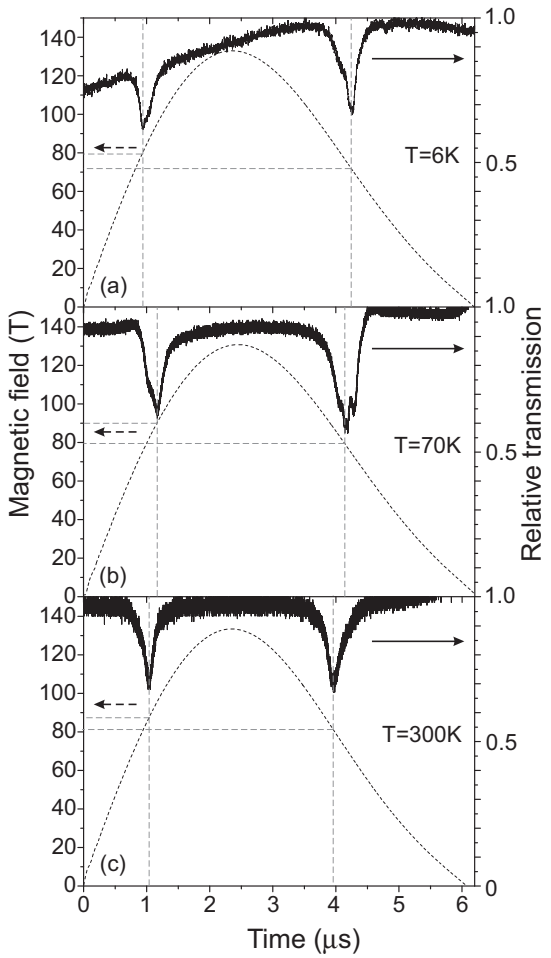

FIG. 1. Optical magnetotransmission (solid curves) and magnetic field intensity (dotted curves) versus time for three temperatures and laser wavelength $\lambda_2 = 9.69\,\mu$m.

coil. The magnetic field induction B was measured at the sample using a dB/dt measuring coil, with an estimated uncertainty not exceeding $\pm 3\%$.

An MQW structure (No. 151) was prepared by means of a low-pressure metal organic vapor phase epitaxy (LP-MOVPE) [38] on the (100) plane semi-insulating GaAs substrates specially for our experiment. It consisted of ten identical GaAs QWs and eleven $Al_xGa_{1-x}As$ barriers. The well thickness was about 10 nm while the width of barriers was about 5 nm. Magnetotransport measurements [33] performed at temperatures from 1.6–4.2 K determined the electron density of 2DEG in MQW investigated of 5×10^{11} cm^{-2} and electron mobility of about 5×10^4 cm^2/Vs.

Magnetotransmission curves versus time recorded for $\lambda_1 = 9.69\,\mu$m at three temperatures (6 K, 70 K, and 300 K) are presented in Figs. 1(a), 1(b), and 1(c), respectively. Magnetic field curves versus time are given on the same figures by dotted curves, which enable us to determine the position of the resonance peaks on the magnetic field scale. Each transmission spectrum has clearly visible resonance minima. The resonance peaks were reproducible while measured for increasing and decreasing magnetic fields. However, shifts to higher magnetic fields were found on curves corresponding to increasing fields.

TABLE I. Positions of resonance fields for increasing and decreasing field runs, as well as average values. The asterisks mark weaker peaks.

T (K)	E (meV)	Incr. peak position (B)	Decr. peak position (B)	Avg. peak position (B)
6	116.7	66	60	63
6	116.7	71	68	69.5
6	116.7	73	70	71.5*
6	116.7	82	80	81*
6	116.7	83	81	82*
6	128.0	75	65	70
6	128.0	81.5	71.5	76.5
6	128.0	84	73	78.5*
6	128.0	89	82	85.5
6	128.0	91	84	87.5*
70	116.7	62	58	60
70	116.7	72	65	68.5
70	116.7	75	67	71
70	116.7	79	71	75
70	116.7	80.5	72.5	76.5*
70	128.0	77	70	73.5*
70	128.0	79	72	75.5
70	128.0	86.5	77.5	81.5
70	128.0	87.5	79.5	83.5
70	128.0	91	83	87.5
70	128.0	92.5	84.5	88.5*
300	116.7	74	71	72.5
300	128.0	87	85	86

This is illustrated in Fig. 1 where the positions of the resonance peaks are attributed to magnetic fields by the additional dashed lines and in Table I where these positions are given exactly. The effect of resonance shifts could be explained by the electron relaxation processes associated with short pulse duration [39]. The values of resonance fields for increasing and decreasing field runs were averaged

$$B_r^{\mathrm{exp}} = \tfrac{1}{2}\left(B_r^{\mathrm{incr}} + B_r^{\mathrm{decr}}\right). \quad (1)$$

In the works of Miura group [1,7], in his experiments on CR at very high magnetic fields in the bulk GaAs single crystals, was shown how temperature affects the structure of resonant peaks. At low temperatures the resonances are dominated by impurity transitions (ICR) related to magnetodonors, as the temperature increases the free-electron transitions begin to dominate. When the source has a fixed radiation frequency, the donor-related transitions occur at lower magnetic fields.

Our results obtained on the MQWs confirms this behavior but an important difference is observed, which is illustrated in Figs. 1–2: at $T = 6$ K the free-electron resonance (marked as CR at about 85 T) is very weak and two ICRs are responsible for magnetooptical transitions in magnetodonors—one stronger at about 70 T [marked as ICR(b)] and a second one at about 78 T [marked as ICR(w)] on the decreasing magnetic field transmission curves. The peaks are split into two, which confirms the approximation of the peaks by two Lorentzians. More visible splitting is observed on curves for decreasing fields at 70 K and $\lambda_2 = 9.69\,\mu$m [see Fig. 2(b)]. Increasing

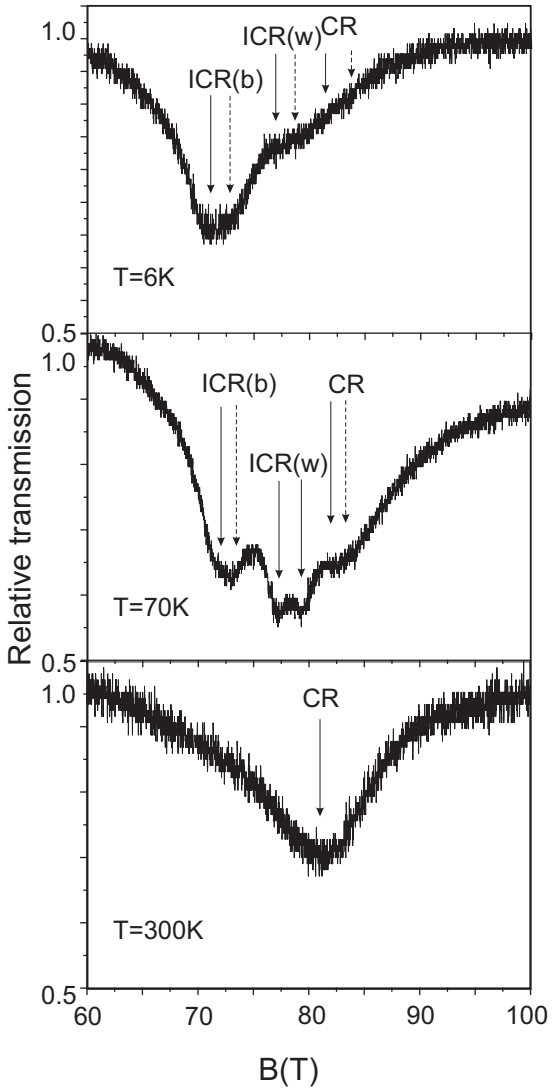

FIG. 2. Resonance curves versus magnetic field for $\lambda_2 = 9.69\,\mu$m at three temperatures obtained at decreased magnetic field. Arrows indicate position ICR and CR peaks, dashed arrows indicate weakly pronounced peaks.

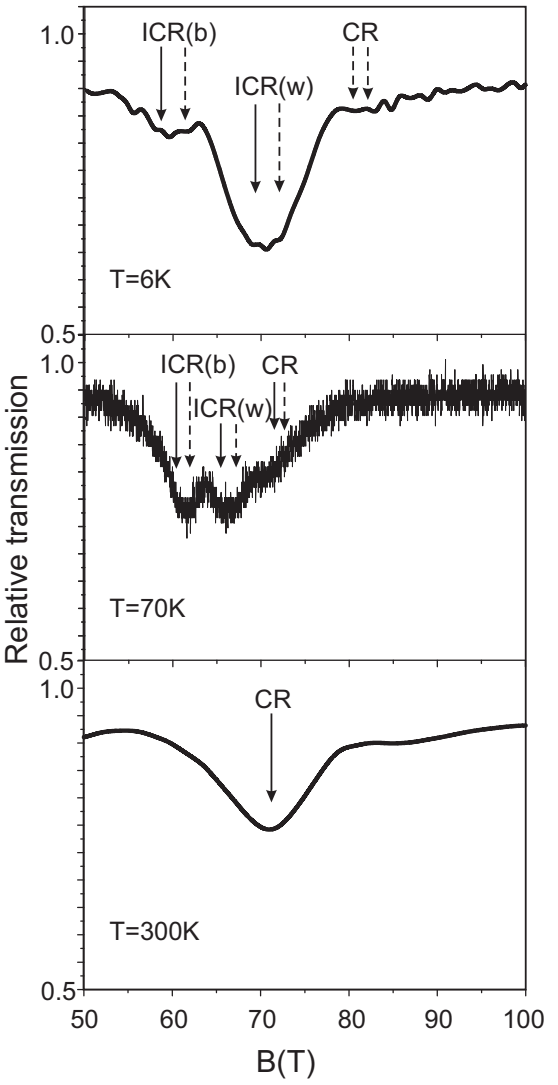

FIG. 3. Resonance curves versus pulsed magnetic field recorded for $\lambda_2 = 10.59\,\mu$m at three temperatures obtained at decreased magnetic field. Arrows indicate positions of ICR and CR peaks, dashed arrows indicate weakly pronounced peaks.

the temperature to 70 K causes ICR(w) at 78 T to become stronger and clearly split while the resonance peak CR at about 83 T (also for decreasing magnetic field) have comparable intensity with ICR. At the temperature 300 K two ICR peaks are disappeared and peak CR is very strong and is shifted to 70 T (moves to the ICR position).

The curves for $\lambda_1 = 10.59\,\mu$m at different temperatures are presented in Fig. 3. One observes the same resonances as those shown in Figs. 1 and 2, but somewhat shifted toward smaller fields. The experimental values of observed resonances for increasing and decreasing fields as well as their averages are presented for both wavelengths in Table I.

III. THEORY

It was shown by magneto-optical studies of the conduction band of GaAs both at low and high magnetic fields that, in addition to the free-electron Landau states, one usually deals in this material with residual Si donors. This is also the case in our studies, as indicated by preliminary inspection of the resonant peaks. They cannot be explained by the free-electron cyclotron resonance alone, also when one takes into account the fact that both $n = 0$ and $n = 1$ Landau levels (LLs) are spin split and, due to band nonparabolicity, the spin splitting of each LL is different. Thus, we have to consider both free-electron and magnetodonor (MD) optical transitions. The free-electron LLs can be described quite precisely including band nonparabolicity and nonsphericity; the description of MD energies is more complicated and we must resort to approximate procedures.

A. Free electrons

The description of free-electron LLs in the nonparabolic and nonspherical conduction band of GaAs was worked out and verified in detail by Pfeffer and Zawadzki [40], so we

will give here only a short summary of this work and use its results. We solve the 14-band $\mathbf{P}\cdot\mathbf{p}$ theory for the bulk material consistently with treating the donor states at high magnetic fields. Finding solutions for the multiple quantum wells would be considerably more complicated and would change the final results very little. One would then count the Landau and donor levels from the lowest multiwell sub-band rather than the wells' bottoms, which would very slightly increase the effect of bands nonparabolicity in GaAs. GaAs is a medium-gap material, so that in order to describe correctly its conduction band it is not enough to apply the standard three-level $\mathbf{P}\cdot\mathbf{p}$ model used for narrow-gap semiconductors. Thus, a five-level $\mathbf{P}\cdot\mathbf{p}$ model is used, which includes in addition two higher conduction levels. One takes at the Γ point of the Brillouin zone two Γ_{15}^{v} valence levels, Γ_{1}^{c} conduction level, and two Γ_{15}^{c} conduction levels. This gives, including degeneracies and spins, 14 states. The initial multiband $\mathbf{P}\cdot\mathbf{p}$ set for carriers in the presence of an external magnetic field is

$$\sum_{l}\left[\left(\frac{\mathbf{P}^2}{2m_0}+E_{l0}-E\right)\delta_{l'l}+\frac{\mathbf{p}_{l'l}\cdot\mathbf{P}}{2m_0}+\mu_B B\cdot\sigma_{l'l}+H_{l'l}^{S.O.}\right]\times f_l=0, \tag{2}$$

where $\mathbf{P}=\mathbf{p}+e\mathbf{A}$ is the kinetic momentum, $\mathbf{A}$ is the vector potential of magnetic field $\mathbf{B}$, E_{l0} are the band-edge energies, $\mathbf{p}_{l'l}$ are the interband matrix elements of momentum, $\sigma_{l'l}$ those of the spin operators and $H_{l'l}^{S.O.}$ those of the spin-orbit interaction. The summation runs over 14 bands. Equation (2) represents a set of coupled differential equations for the envelope functions f_l. Far-band contributions are included using the perturbation theory up to the P^2 terms. If the considered energy bands were spherical, one could find solutions of the set (2) by a column of single harmonic oscillator functions. However, an interaction of the two higher conduction levels with the two lowest valence levels of the set results in a slight nonsphericity of the bands, including the Γ_6^c conduction band of our interest. To account for this feature, one looks for solutions of the problem (2) in the form of sums of harmonic oscillator functions [41]. It turns out that LLs have somewhat different energies for [001], [110], [111] field orientations. This is of particular importance for the spin splittings, which can change signs from negative to positive as the magnetic field increases. When computing energies we have to use the material parameters for the five-level model. We take the conduction band-edge values of $m_0^*=0.066m_0$ and $g_0^*=-0.44$, as determined by the cyclotron and spin resonances. The mass value includes the so-called polaron contribution, i.e., the effect of nonresonant electron-polar phonon interaction. This interaction increases the effective mass at low magnetic fields according to the relation

$$m^*(\exp)=m_0^*\left(1-\frac{\alpha}{6}\right)^{-1}, \tag{3}$$

where α is the polar coupling constant. Knowing the value of $\alpha=0.085$ and the experimentally measured mass $m^*(\exp)$, one determines the bare mass $m_0^*=0.0651m_0$, which should be used in the Landau level calculations for very high magnetic fields at which the optic phonons do not contribute. We use the following values of experimental gaps: $E_0=-1.519\,\mathrm{eV}$ and the matrix elements of momentum: $E_{P_0}=27.86\,\mathrm{eV}$, in the standard units $E_P=2m_0P^2/\hbar^2$. The Luttinger valence-band parameters resulting from the interaction of far bands with the Γ_{15}^{v} bands are [40]: $\gamma_1^L=7.80$, $\gamma_2^L=2.46$, $\gamma_3^L=3.30$, $\kappa^L=2.03$.

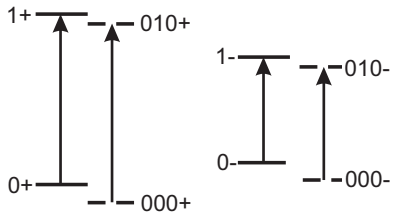

FIG. 4. Cyclotron resonance and MD cyclotron resonance transitions for both spin orientation. It is seen that for the LL number of 0 the 0− is higher as 0+ and in the case of LL number 1 is contrary the 1+ is higher as 1−.

The basic matrix that has to be computed for a given LL n and specific spin orientation has dimensions 7×7. However, the basic 7×7 matrices for different n are coupled by the nonspherical terms into matrices of higher dimensions. In order to obtain the sufficient precision for the field $\mathbf{B}\parallel[001]$ we truncate the matrices at the dimension 35×35 and compute their eigenenergies. Going to higher-order matrices corresponds to including higher orders of bands nonsphericity, which affects the computed level energies very little, see for details Ref. [40] . The calculated energies exhibit nonlinear dependence of LLs on B due to band nonparabolicity. The most striking feature is the change of spin splitting from negative at low fields (expressed by the negative values of spin g factors) to positive at high fields. The change of sign occurs at lower B intensities for LLs with higher n, see Ref. [40]. This is illustrated schematically in Fig. 4, which shows that for $n=0$ the g value is negative (0+ state is lower than 0−), while for $n=1$ the g value is positive (1− state is lower than 1+). In the calculations we do not change the energy gap of GaAs for temperatures between 6 K and 70 K because, as follows from Ref. [42], the change of energy gap due to dilatation in this material is negligible in the low-temperature range.

B. Magnetodonors

In order to treat magnetodonor (MD) energies at the comparable level of precision, one would need to write down the donor potential in the 14 diagonal terms of the initial matrix (2) and deal with the resulting eigenvalue problem. This is not a tractable task, so we have to resort to approximate solutions. A key parameter in the MD problem is ratio of the binding donor energy to the magnetic energy, i.e.,

$$\gamma=\frac{h\omega_c}{2Ry^*}, \tag{4}$$

where $\omega_c=eB/m_0^*$ and $Ry^*=m^*e^4/2\kappa^2\hbar^2$ is the effective Rydberg. In GaAs there is $Ry^*=5.9\,\mathrm{meV}$, so that at a magnetic field of B 86 T we have $\gamma=13.6$. It follows from the work of Brozak *et al.* [36] that at values $\gamma>6$ one can treat the MD problem in a quantum well with the magnetic field perpendicular to the interfaces, i.e., in the Faraday

configuration, as a problem in the bulk. This considerably facilitates our task.

We want to solve the MD problem using variational procedure. Since the formalism of 14×14 matrix is not tractable for this purpose, we imitate the nonparabolicity of the conduction band by employing a two-band model with an effective energy gap ϵ_g^*. Thus, we take the effective gap value, which gives the same nonparabolicity as the 14×14 band procedure. It was shown in Ref. [7] that the value of such a gap for GaAs is 0.98 eV. Then the two-band equation (omitting spin) is

$$E = \frac{-\epsilon_g^*}{2} + \left[\left(\frac{\epsilon_g^*}{2}\right)^2 + \epsilon_g^* \langle K \rangle\right]^{1/2} + \langle U \rangle, \tag{5}$$

where the variational averages of kinetic and potential parts of the MD energy are, correspondingly (in the cylindrical coordinate system)

$$\langle K \rangle = \langle \Psi_{NM\beta} | -\nabla^2 - i\gamma \frac{\partial}{\partial \varphi} + \frac{\gamma^2 \rho^2}{4} | \Psi_{NM\beta} \rangle, \tag{6}$$

$$\langle U \rangle = \langle \Psi_{NM\beta} | \frac{-2}{(\sqrt{z^2 + \rho^2})} | \Psi_{NM\beta} \rangle. \tag{7}$$

The energies are in effective Rydbergs and lengths in the effective Bohr radii. The potential energy in Eq. (5) stands outside the square root since, in the multiband $\mathbf{P}\cdot\mathbf{p}$ matrix, the potential always appears in diagonal terms together with the energy. One calculates the variational averages of $\langle U \rangle$ and $\langle K \rangle$ and than minimizes the energy of Eq. (5). However, we cannot hope to get sufficiently precise absolute MD energies from the above variational and simplified band structure procedures to be compared with the precise free-electron energies. For this reason we calculate from Eq. (5) only shifts of the MD energies, as counted from the free-electron energies. The calculation of the shifts amounts to separate evaluation of the variational energies according to Eq. (5) and their comparison with the free-electron energies according to the same two-band model, by putting in Eq. (5) $\langle U \rangle = 0$ and $\langle K \rangle = 2\gamma(n + 1/2)$, i.e., the energy of free-electron LL n.

As to spin contributions to the energies, the two-band equation of the type (5) can not reproduce the change of signs of the spin splittings mentioned above. In this situation, we assume that the spin splitting of MD energies is the same as that of the free-electron energies calculated from the 14×14 scheme. Thus, in order to obtain the complete MD energies, we shift the calculated free-electron Landau levels (which include the spin) by the above-mentioned amounts not depending on the spin. The assumption of identical spin splittings for LLs and MD energies is well justified since the energy differences between free and bound electron states are much smaller than their absolute energies at high fields. Since we deal with very high magnetic fields, expressed by the high values of γ, we can use one-parameter trial functions proposed by Wallis and Bowlden [43] in the variational calculations of MD energies. These functions express the fact that, in the MD state, the component of the motion transverse to magnetic field is almost equal to that of the magnetic radius for a free-electron, so that one varies only the longitudinal component [4]:

$$\Psi_{NM\beta} = C \cdot e^{i \cdot M \cdot \Phi} e^{-\frac{\rho}{2}} \rho^{-\frac{|M|}{2}} L_N^M(\rho) P_\beta(z) e^{-\frac{1}{4}\gamma\lambda z^2}. \tag{8}$$

Here λ is variational parameter, L_N^M are associated Laguerre polynomials and $P_\beta(z)$ are orthogonal polynomials. The quantum numbers are: $N = 0,1,2,\ldots, M = -2,-1,0,1,2,\ldots, \beta = 0,1,2,\ldots$. Taking the trial functions with higher negative M would result in higher absolute values of variational energies. However, in the variational procedure, the lower computed energy is always closer to the exact value. We need only $P_0(z) = (\gamma\lambda/2\pi)^{(1/4)}$. The Landau level number to which a given MD state belongs is $n = N + 1/2(M + |M|)$. For the MD states of our interest we take explicitly

$$\Psi_{000} = C \cdot e^{-\frac{\rho}{2}+1} \rho L_0^0(\rho) \left(\frac{\gamma\lambda}{2\pi}\right)^{\frac{1}{4}} e^{-\frac{1}{4}\gamma\lambda z^2} \tag{9}$$

$$\Psi_{010} = C \cdot e^{i\varphi} e^{-\frac{\rho}{2}+1} \rho^{-\frac{1}{2}} L_0^1(\rho) \left(\frac{\gamma\lambda}{2\pi}\right)^{\frac{1}{4}} e^{-\frac{1}{4}\gamma\lambda z^2}, \tag{10}$$

where $L_0^0(\rho) = L_0^1(\rho) = 1$. The normalization coefficients C and the variational parameters λ are different for each function. Thus, the complete theory includes in the first step precise calculation of the free-electron energies with the use of 14×14 $\mathbf{P}\cdot\mathbf{p}$ formalism. These are directly used to interpret the free-electron data. Next, we calculate variational MD energies from the two-band equation (5) with the effective energy gap and calculate the MD energy shifts using the same two-band equation (5) for free electrons with the same effective gap. Finally, the obtained shifts are subtracted from the exactly calculated free-electron energies and used to interpret the experimental results for magnetodonors.

IV. COMPARISON OF EXPERIMENT WITH THEORY

In Fig. 5 we show all observed resonance points and lines calculated according to the presented theory for magneto-optical transitions between the free-electron LLs $n = 0$ and $n = 1$, as well as MD states (000) and (010). The spin splittings are calculated for free electrons, as explained above. Experimental positions of the observed resonances at 6 K are indicated by black squares. It is seen that the observed central stronger peak should be attributed to the transition between the MD states. The uncertainties of our experimental points

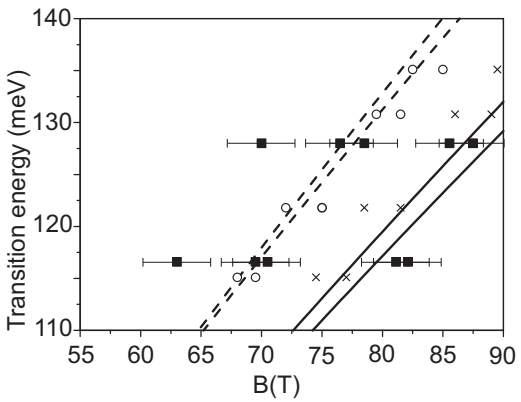

FIG. 5. Magneto-optical transition energies calculated including spin splitting according to theory presented in Sec. III and experimental data obtained at 6 K: full squares are our data, circles and crosses are data of Ref. [7].

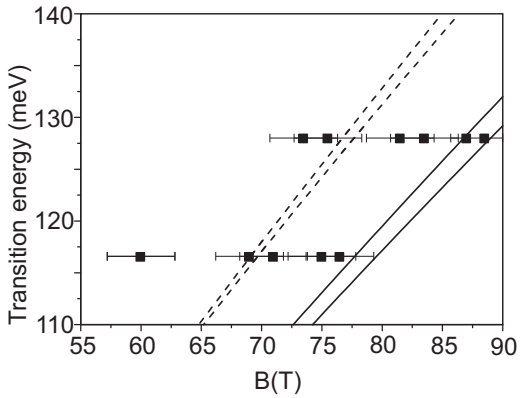

FIG. 6. Positions of resonance peaks at 70 K for wavelengths λ_1 and λ_2 and theoretical lines versus magnetic field.

are determined by different resonance positions for increasing and decreasing field runs, as indicated in Table I. In general, the agreement between our experiment and theory is quite good for both LL and MD spin doublets shown in Fig. 5. The spin g value for conduction electrons in GaAs is known to be very small, but at our very high magnetic field it results in sizable splittings. The data show that the spin splittings of LL and MD transitions are quite similar indicating that our assumption in this respect was reasonable. Finally, a good agreement of experiment and theory for free-electron transitions confirms indirectly but convincingly that, indeed, the polaron corrections to the effective electron mass are absent at high magnetic fields.

There appear two additional resonances [ICR(b)] on the lower field side whose origin is not clear. Huant *et al.* [3,5,6,44] observed in GaAs/AlGaAs quantum wells magneto-optical transitions ascribed to donors in AlGaAs barriers [3,5,44,45]. According to calculations [44] and observations reported in Ref. [45] the energies of transitions for MD in barriers are slightly higher than the cyclotron resonance. This would correspond in our experiments with fixed laser frequencies to resonances on weaker field sides, in agreement with our observations. On the other hand, the MD donors in the center of a barrier have distinctly smaller transition energies than those in the center of a well. Because donors in our MQW are in wells and barriers we presume that these resonances correspond to optical transitions of electrons in barriers.

The weak minimum recorded at higher magnetic fields, as it is seen from Figs. 1– 3 is caused by CR in QW although agreement with the theoretical position of this resonance is worse. The temperature dynamic of observed peaks confirms this interpretation while, at higher temperature (70 K, see Figs. 1– 3) this peak is stronger and at 300 K it becomes a single peak. Resonance recorded from the smaller fields at 70 K (see Fig. 4) should be referred to the MD transitions in barriers. The reduced nonionized donors in barriers cause these transitions as it has been shown in Refs. [3,5,44] in the region of smaller magnetic fields. In the case of the MD transitions in the AlGaAs barriers the spin splitting is smaller and is outside experimental resolution of 1.5 T. In Fig. 6 we show the data taken at $T = 70$ K and unchanged theoretical lines. There appears a doublet for the higher frequency between the theoretical lines whose origin is unclear. In principle, higher temperatures activate free-electron transitions but there are no free-electron states to produce this doublet. There is one resonance at lower magnetic fields, similar to those indicated in Fig. 5. Nevertheless, we find that the overall agreement between the experiment and theory is quite reasonable, confirming our simplified treatment of magnetodonor energies. There appear few additional unexplained resonances, which can be attributed to inhomogeneous character of multiple GaAs/AlGaAs quantum wells doped with Si.

V. SUMMARY

Very high pulsed magnetic fields up to 140 T were used to study cyclotron resonance and magnetodonor optical transitions in multiple GaAs/AlGaAs quantum wells in the Faraday configuration. The magneto-optical spectra taken at $T = 6, 70$, and 300 K exhibit different details as the temperature changes. The observed free-electron magneto-optical transitions were described by the $\mathbf{P}\cdot\mathbf{p}$ theory including 14 energy bands that account for the nonparabolicity and nonsphericity of the conduction band in GaAs. Shifts of magnetodonor energies with respect to the free-electron energies were calculated by a variational procedure taking into account effective nonparabolicity of the conduction band in GaAs. The applied theory successfully describes our data, as well as data of other authors quoted for comparison. A possible origin of a few unexplained resonances [ICR(b)] is discussed. Our study confirms the general picture of both free-electron and magnetodonor states in GaAs/AlGaAs multiple quantum wells in a very wide range of magnetic fields, which is important for various applications.

ACKNOWLEDGMENTS

This work is supported by National Science Foundation - Cooperative Agreement No. DMR-1157490, the State of Florida, and the U.S. Department of Energy. We are grateful to NSF and LANL for the opportunity to perform the CR experiment.

[1] S. P. Najda, S. Takeyama, N. Miura, P. Pfeffer, and W. Zawadzki, Phys. Rev. B **40**, 6189 (1989).
[2] D. M. Larsen, Phys. Rev. B **44**, 5629 (1991).
[3] S. Huant, S. P. Najda, and B. Etienne, Phys. Rev. Lett. **65**, 1486 (1990).
[4] W. Zawadzki, in *Landau Level Spectroscopy*, edited by G. Landwehr and E. I. Rashba (North-Holland, Amsterdam, 1991), pp. 679–776.
[5] S. Huant, A. Mandray, and B. Etienne, Phys. Scr. **T45**, 145 (1992).

[6] S. Huant, A. Mandray, J. Zhu, S. G. Louie, T. Pang, and B. Etienne, Phys. Rev. B **48**, 2370 (1993).

[7] W. Zawadzki, P. Pfeffer, S. P. Najda, H. Yokoi, S. Takeyama, and N. Miura, Phys. Rev. B **49**, 1705 (1994).

[8] J. P. Cheng, Y. J. Wang, B. D. McCombe, and W. Schaff, Phys. Rev. Lett. **70**, 489 (1993).

[9] A. B. Dzyubenko, A. Mandray, S. Huant, A. Y. Sivachenko, and B. Etienne, Phys. Rev. B **50**, 4687 (1994).

[10] J. Frigerio, P. Chaisakul, D. Marris-Morini, S. Cecchi, M. S. Roufied, G. Isella, and L. Vivien, Appl. Phys. Lett. **102**, 061102 (2013).

[11] T. A. Krajewski, K. Dybko, G. Luka, E. Guziewicz, P. Nowakowski, B. S. Witkowski, R. Jakiela, L. Wachnicki, A. Kaminska, A. Suchocki, and M. Godlewski, Acta Mater. **65**, 69 (2014).

[12] G. Pica, G. Wolfowicz, M. Urdampilleta, M. L. W. Thewalt, H. Riemann, N. V. Abrosimov, P. Becker, H.-J. Pohl, J. J. L. Morton, R. N. Bhatt, S. A. Lyon, and B. W. Lovett, Phys. Rev. B **90**, 195204 (2014).

[13] A. J. Sigillito, R. M. Jock, A. M. Tyryshkin, J. W. Beeman, E. E. Haller, K. M. Itoh, and S. A. Lyon, Phys. Rev. Lett. **115**, 247601 (2015).

[14] M. O. Manasreh and G. L. McCoy, *Semiconductor Quantum Wells and Superlattices for Long-Wavelength Infrared Detectors* (ARTECH, Boston, 1993).

[15] S. M. Ramey and R. Khoie, IEEE Trans. Electron Devices **50**, 1179 (2003).

[16] L. Hoglund, K. F. Karlsson, P. O. Holtz, H. Pettersson, M. E. Pistol, Q. Wang, S. Almqvist, C. Asplund, H. Malm, E. Petrini, and J. Y. Andersson, Phys. Rev. B **82**, 035314 (2010).

[17] M. Zaluny, Phys. Rew. B **91**, 035303 (2015).

[18] C. Chen, N. Braidy, C. Couteau, C. Fradin, G. Weihs, and R. LaPierre, Nano Lett. **8**, 495 (2008).

[19] L. Rigutti, A. Castaldini, and A. Cavallini, Phys. Rev. B **77**, 045312 (2008).

[20] J. R. Riley, S. Padalkar, Q. Li, P. Lu, D. D. Koleske, J. J. Wierer, G. T. Wang, and L. J. Lauhon, Nano Lett. **13**, 4317 (2013).

[21] N. Wang, L. Cheng, R. Ge, S. Zhang, Y. Miao, W. Zou, C. Yi, Y. Sun, Y. Cao, R. Yang, Y. Wei, Q. Guo, Y. Ke, M. Yu, Y. Jin, Y. Liu, Q. Ding, D. Di, L. Yang, G. Xing, H. Tian, C. Jin, F. Gao, R. H. Friend, and J. Wang, Nature Photon. **10**, 699 (2016).

[22] M. Załużny, Phys. Rev. B **43**, 4511 (1991).

[23] F. Szmulowicz, M. O. Manasreh, C. E. Stutz, and T. Vaughan, Phys. Rev. B **50**, 11618 (1994).

[24] J. Faist, F. Capasso, D. L. Sivco, C. Sirtori, A. L. Hutchinson, and A. Y. Cho, Science **264**, 553 (1994).

[25] P. Rauter, T. Fromherz, N. Q. Vinh, B. N. Murdin, G. Mussler, D. Grutzmacher, and G. Bauer, Phys. Rev. Lett. **102**, 147401 (2009).

[26] J. Lee, M. Tymchenko, C. Argyropoulos, P.-Y. Chen, F. Lu, F. Demmerle, G. Boehm, M.-C. Amann, A. Al, and M. A. Belkin, Nature (London) **511**, 65 (2014).

[27] A. V. Poshakinskiy, A. N. Poddubny, and A. Fainstein, Phys. Rev. Lett. **117**, 224302 (2016).

[28] D. Huang and M. O. Manasreh, Phys. Rev. B **54**, 2044 (1996).

[29] C. Negrevergne, T. S. Mahesh, C. A. Ryan, M. Ditty, F. Cyr-Racine, W. Power, N. Boulant, T. Havel, D. G. Cory, and R. Laflamme, Phys. Rev. Lett. **96**, 170501 (2006).

[30] D. Ploch, E. M. Sheregii, M. Marchewka, M. Wozny, and G. Tomaka, Phys. Rev. B **79**, 195434 (2009).

[31] M. Marchewka, E. M. Sheregii, I. Tralle, A. Marcelli, M. Piccinini, and J. Cebulski, Phys. Rev. B **80**, 125316 (2009).

[32] M. Marchewka, E. M. Sheregii, I. Tralle, D. Płoch, G. Tomaka, M. Furdak, A. Kolek, A. Stadler, K. Mleczko, D. Żak, W. Strupiński, A. Jasik, and R. Jakieła, Physica E (Amsterdam) **40**, 894 (2008).

[33] M. Zybert, M. Marchewka, G. Tomaka, and E. M. Sheregii, Physica E (Amsterdam) **44**, 2056 (2012).

[34] X. Wu, M. Tuan Trinh, and X. Y. Zhu, J. Phys. Chem. C **119**, 14714 (2015).

[35] H. Fang, H. A. Bechtel, E. Plis, M. C. Martin, S. Krishna, E. Yablonovitch, and A. Javey, Proc. Nat. Acad. Sci. USA **110**, 11688 (2013).

[36] G. Brozak, B. D. McCombe, and D. M. Larsen, Phys. Rev. B **40**, 1265 (1989).

[37] L. G. Booshehri, C. H. Mielke, D. G. Rickel, S. A. Crooker, Q. Zhang, L. Ren, E. H. Haroz, A. Rustagi, C. J. Stanton, Z. Jin, Z. Sun, Z. Yan, J. M. Tour, and J. Kono, Phys. Rev. B **85**, 205407 (2012).

[38] A. Jasik, A. Wnuk, J. Gaca, M. Wójcik, A. Wójcik-Jedlinska, J. Muszalski, and W. Strupiński, J. Cryst. Growth **311**, 4423 (2009).

[39] S. Hansel, C. Puhle, M. von Ortenberg, and E. Huseynov, Physica B (Amsterdam) **346-347**, 479 (2004).

[40] P. Pfeffer and W. Zawadzki, Phys. Rev. B **53**, 12813 (1996).

[41] V. Evtuhov, Phys. Rev. **125**, 1869 (1962).

[42] W. Zawadzki, P. Pfeffer, R. Bratschitsch, Z. Chen, S. T. Cundiff, B. N. Murdin, and C. R. Pidgeon, Phys. Rev. B **78**, 245203 (2008).

[43] R. F. Wallis and H. J. Bowlden, J. Phys. Chem. Solids **7**, 78 (1958).

[44] S. Huant, A. Mandray, and B. Etienne, Solid State Commun. **93**, 435 (1995).

[45] E. Glaser, B. V. Shanabrook, R. L. Hawkins, W. Beard, J.-M. Mercy, B. D. McCombe, and D. Musser, Phys. Rev. B **36**, 8185(R) (1987).